

2015

Interfacial electronic structure at the CH₃NH₃PbI₃/MoO_x interface

Peng Liu
Central South University

Xiaoliang Liu
Central South University, xl_liu@csu.edu.cn


Lu Lyu
Central South University

Haipeng Xie
Central South University

Hong Zhang
Central South University

See next page for additional authors

Follow this and additional works at: <http://digitalcommons.unl.edu/mechengfacpub>

 Part of the [Mechanical Engineering Commons](#), and the [Physical Sciences and Mathematics Commons](#)

Liu, Peng; Liu, Xiaoliang; Lyu, Lu; Xie, Haipeng; Zhang, Hong; Niu, Dongmei; Huang, Han; Bi, Cheng; Xiao, Zhengguo; Huang, Jinsong; and Gao, Yongli, "Interfacial electronic structure at the CH₃NH₃PbI₃/MoO_x interface" (2015). *Mechanical & Materials Engineering Faculty Publications*. 118.
<http://digitalcommons.unl.edu/mechengfacpub/118>

This Article is brought to you for free and open access by the Mechanical & Materials Engineering, Department of at DigitalCommons@University of Nebraska - Lincoln. It has been accepted for inclusion in Mechanical & Materials Engineering Faculty Publications by an authorized administrator of DigitalCommons@University of Nebraska - Lincoln.

Authors

Peng Liu, Xiaoliang Liu, Lu Lyu, Haipeng Xie, Hong Zhang, Dongmei Niu, Han Huang, Cheng Bi, Zhengguo Xiao, Jinsong Huang, and Yongli Gao

Interfacial electronic structure at the $\text{CH}_3\text{NH}_3\text{PbI}_3/\text{MoO}_x$ interface

Peng Liu,¹ Xiaoliang Liu,^{1,a)} Lu Lyu,¹ Haipeng Xie,¹ Hong Zhang,¹ Dongmei Niu,¹ Han Huang,¹ Cheng Bi,² Zhengguo Xiao,² Jinsong Huang,² and Yongli Gao^{3,a)}

¹*Institute of Super-Microstructure and Ultrafast Process in Advanced Materials, College of Physics and Electronics, Central South University, Changsha 410083, People's Republic of China*

²*Department of Mechanical and Materials Engineering and Nebraska Center for Materials and Nanoscience, University of Nebraska-Lincoln, Lincoln, Nebraska 68588-0656, USA*

³*Department of Physics and Astronomy, University of Rochester, Rochester, New York 14627, USA*

(Received 25 March 2015; accepted 5 May 2015; published online 15 May 2015)

Interfacial electronic properties of the $\text{CH}_3\text{NH}_3\text{PbI}_3$ (MAPbI_3)/ MoO_x interface are investigated using ultraviolet photoemission spectroscopy and X-ray photoemission spectroscopy. It is found that the pristine MAPbI_3 film coated onto the substrate of poly (3,4-ethylenedioxythiophene) poly(styrenesulfonate)/indium tin oxide by two-step method behaves as an n-type semiconductor, with a band gap of ~ 1.7 eV and a valence band edge of 1.40 eV below the Fermi energy (E_F). With the MoO_x deposition of 64 Å upon MAPbI_3 , the energy levels of MAPbI_3 shift toward higher binding energy by 0.25 eV due to electron transfer from MAPbI_3 to MoO_x . Its conduction band edge is observed to almost pin to the E_F , indicating a significant enhancement of conductivity. Meanwhile, the energy levels of MoO_x shift toward lower binding energy by ~ 0.30 eV, and an interface dipole of 2.13 eV is observed at the interface of $\text{MAPbI}_3/\text{MoO}_x$. Most importantly, the chemical reaction taking place at this interface results in unfavorable interface energy level alignment for hole extraction. A potential barrier of ~ 1.36 eV observed for hole transport will impede the hole extraction from MAPbI_3 to MoO_x . On the other hand, a potential barrier of ~ 0.14 eV for electron extraction is too small to efficiently suppress electrons extracted from MAPbI_3 to MoO_x . Therefore, such an interface is not an ideal choice for hole extraction in organic photovoltaic devices. © 2015 AIP Publishing LLC. [<http://dx.doi.org/10.1063/1.4921339>]

Recently, organometal halide perovskite materials such as methylammonium lead halides ($\text{CH}_3\text{NH}_3\text{PbX}_3$, X = I, Cl, Br) have arisen as one of the most attractive candidates for producing solar cells due to their high efficiency, cheap and abundant raw materials, and good scalability for industrial production.^{1–8} Kojima *et al.*⁹ first reported in 2009 on a 3.8% efficient solar cell with perovskite $\text{CH}_3\text{NH}_3\text{PbI}_3$ (MAPbI_3) and TiO_2 . Grätzel *et al.*¹⁰ brought the efficiency to 15% by depositing PbI_2 on nanoporous TiO_2 and subsequently submerging it into a $\text{CH}_3\text{NH}_3\text{I}$ (MAI) solution. Using vapor deposition, Snaith's group¹¹ demonstrated that a planar heterojunction MAPbI_3 solar cell, without the mesoporous electrode in typical sensitized solar cells, could have very high efficiency of 15%. Yang's team¹² achieved an efficiency of 19.3% in MAPbI_3 solar cells by controlling the formation of the MAPbI_3 layer and careful choice of other materials. It is expected that the efficiency of 20% or higher can be reached by optimizing the device structures. The high performance of perovskite based solar cells had been partly ascribed to its very long carrier diffusion lengths by many authors. Snaith's group¹³ reported a diffusion length exceeding 1 μm in a MAPbI_3 absorber. Huang's group¹⁴ observed an electron-hole diffusion length of over 170 μm in solution-grown MAPbI_3 single crystals.

Many efforts have also been made to improve the charge transport and collection at the electrodes in organic devices. Transition metal oxide MoO_x has been extensively used as an insertion layer between the anode and the organic active

materials in organic photovoltaic (OPV) cells^{15–20} and organic light emitting diodes (OLED).^{21–23} The high work function (WF) of MoO_x usually leads the highest occupied molecular orbital (HOMO) level of the contact organics bending-up toward the interface, which reduces the interface potential barrier and facilitates the hole extraction or injection at the interface. The encouraging performance enhancement has been demonstrated by many authors in small molecule OPV cells. Kröger *et al.*²⁴ proposed that the MoO_x interlayer at the anode tremendously enhanced hole injection into organic layer via electron extraction from the HOMO of organic layer through the MoO_x conduction band. Nakayama *et al.*²⁵ further inferred the origin of the hole injection enhancement by the MoO_x insertion layer. This line of work has recently been summarized by Wang *et al.*²⁶ Furthermore, MoO_x has also been demonstrated effective as an anode insertion layer in inorganic thin layer photovoltaic devices (IPV).²⁷ It is therefore highly desirable to investigate if MoO_x may serve the same role in perovskite based solar cells.

Here, we report our effort in investigating a $\text{MAPbI}_3/\text{MoO}_x$ interface, and addressing its electronic structure to verify whether or not such an interface is a potential candidate to enhance efficiently hole extraction in perovskite devices as in OPVs. Ultraviolet photoemission spectroscopy (UPS) and X-ray photoemission spectroscopy (XPS) data were collected as MoO_x was deposited layer by layer on MAPbI_3 film, and the interfacial chemistry and energy level alignment were measured to determine whether a deposited MoO_x insertion layer might serve as an injection/extraction layer between the anode and active layer as the case in OPVs. Our results

^{a)}Electronic addresses: xl_liu@csu.edu.cn and ygao@pas.rochester.edu

indicate, however, the lack of chemical stability of the MAPbI₃ manifested by the strong interface reaction when MoO_x is deposited onto the MAPbI₃, as well as the energy levels mismatch between the MoO_x and the MAPbI₃, makes it not directly suitable for such insertion layers to be effective in MAPbI₃ based solar cells.

The MAPbI₃ film was fabricated by a two-step interdiffusion of spin-coated stacking layers of PbI₂ and MAI. Details about the MAPbI₃ film fabrication could be found elsewhere^{28,29} We evaporated MoO_x layers on MAPbI₃ gradually and the thickness of the MoO_x film increased from submonolayer (0.5 Å) to several atom layers (64 Å) at a controlled rate of 0.2–0.3 Å/min were monitored by a quartz thickness monitor. At each MoO_x film thickness, we measured UPS and XPS spectra to learn the energy level alignment and interface reaction. The UPS was measured with He I (21.22 eV) and XPS with standard Al K_α X-ray source (1486.6 eV). A total energy resolution of 70 meV was selected for the UPS measurements as determined from the Fermi edge of Au. For XPS, the pass energy of the spectrometer with a resolution of 0.5 eV was 40 eV. The binding energies of all UPS and XPS spectra were calibrated and referenced to the Fermi level (E_F) of the analyzer. All measurements were taken at room temperature.

Shown in Figure 1 are the UPS spectra of evaporated MoO_x films on MAPbI₃ substrate. Figure 1(a) displays the evolution of secondary photoemission cut-off with the gradual deposition of MoO_x layers, from which we can know the WF of the sample surface. The WF was obtained from the energy difference between the secondary cut-off and the E_F of the system. For as-grown MAPbI₃, the WF was measured to be 4.13 eV, a little larger than other groups' reports.³⁰ It increased to 4.59 eV with the subsequent MoO_x deposition of 0.5 Å on MAPbI₃. Then it increased gradually, and finally saturated at 6.65 eV with the MoO_x deposition of 64 Å, resulting in a total WF increase of 2.52 eV. Interestingly, there was a sharp increase of WF between 4 Å and 12 Å,

which could be possibly associated with a fully qualified MoO_x molecular layer formed at a certain thickness in this range. Figure 1(b) presents the UPS data of the highest lying valence band (VB) regions, in which the VB maximum (VBM) of MAPbI₃ film displays ~1.40 eV. A characteristic VB peak of MoO_x could be distinguished beyond a MoO_x coverage of 12 Å with the formation of a complete molecular layer of MoO_x. However, a shoulder peak was observed at ~4.43 eV with the MoO_x deposition of up to 1 Å, indicating a MoO_x VBM of 3.09 eV. With the subsequent deposition of up to 64 Å, the VBM shifted upward (to E_F) and finally saturated at about 2.78 eV, which indicated a total shift upward of ~0.3 eV.

To highlight the effect of the MoO_x thickness on the energy level shift, the detailed evolutions of the WF and VBM are shown in Figure 1(c) as the MoO_x thickness increases. It is clear that the WF and VBM change more rapidly until the MoO_x deposition of 16 Å; and then the changes become gradual at the following steps; finally, with the MoO_x deposition of over 32 Å, the shifts practically saturate. The shift of WF can be ascribed to the contributions of interface dipole and band-bending. The upward band-bending of the MoO_x VBM may be ascribed to less oxygen deficiencies in thicker MoO_x coverages than in thinner MoO_x ones, leading to a change from MoO_x⁻ to neutral MoO_x. It is consistent with our XPS data to be presented later, in which more Mo⁶⁺ was detected in thicker MoO_x coverages. Furthermore, it should be noted that at the first several steps, the ionization potential (IP) of MoO_x presents an upward tendency, which is associated with the chemical reaction in the interface region, in which the I component is reduced, possibly by passing the electron to MoO_x and becoming neutral. This can lead to the formation of volatile I that in turn escapes to the vacuum, resulting in the interface region no longer pure MAPbI₃.

In order to gain a better understanding of the energy levels evolution and the interface reaction, we used XPS to

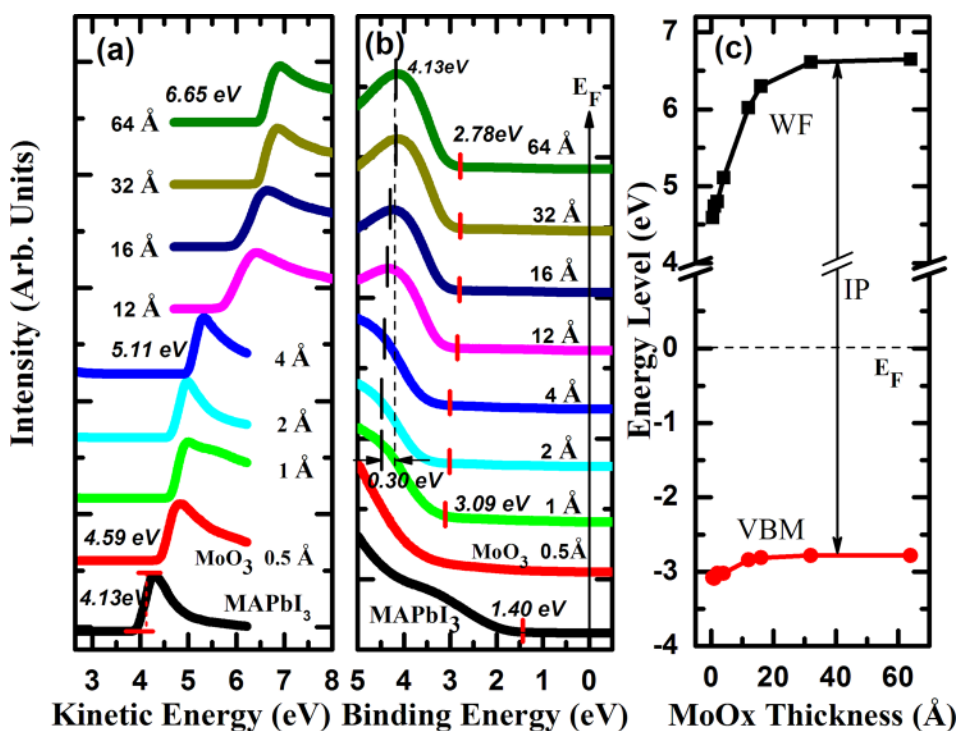


FIG. 1. Thickness dependent UPS data of MoO_x on MAPbI₃ film showing (a) the cut-off region and (b) the VBM region. (c) The evolution of WF and VBM as increasing the MoO_x thickness.

investigate further the chemical characteristics. Shown in Figure 2 are the XPS spectra of Pb 4f_{7/2}, I 3d_{5/2}, Mo 3d, and O 1s core levels in the MAPbI₃/MoO_x interface as the MoO_x coverage increases. All the spectra were normalized to the same height for visual clarity. The information of the elements in MAPbI₃ substrate is just presented for low overlayer of MoO_x (up to 16 Å) due to the limit of XPS probing depth. From Figure 2(a), we can find that the Pb 4f_{7/2} core level comprises two components represented by two peaks which center on 138.59 eV and 136.80 eV, respectively. The bigger one (centered on 138.59 eV) can be associated to the Pb component in MAPbI₃, while the smaller one to the little metallic Pb decomposed from MAPbI₃, most likely due to the chemical reaction and sample annealing before the deposition of MoO_x film on it.³¹ With the deposition of MoO_x on the MAPbI₃ substrate, both of the two peaks shift toward higher binding energies during the initial several steps of MoO_x deposition, accompanied with sharp intensity reduction. The total shift of Pb 4f_{7/2} is measured to be ~0.4 eV before it reaches saturation. Almost the same shift can be

obtained for I 3d in Figure 2(b), which indicates a downward band bending of 0.4 eV in the energy levels of the MAPbI₃ film. However, the actual band bending should be rectified by incorporating the charging effect during the XPS measurement, which will be discussed further below. The C 1s spectrum of the pristine MAPbI₃ substrate (not showing here) mainly consists of two kinds of carbon components at 286.78 eV and 285.10 eV, respectively. The one at 286.78 eV (72%) can be attributed to the well-ordered and stoichiometric MAPbI₃, and the other (28%) from carbon impurities.

Shown in Figures 2(c) and 2(d) is the evolution of Mo 3d and O 1s XPS peaks, respectively. As a multivalence element, Mo has oxidation states 5+ and 6+ in our MoO_x film. The evaporated MoO_x films had been observed to be heavily n-type doped due to the oxygen deficiency³² as we discussed previously. The difference of stoichiometric MoO₃ versus oxygen deficient MoO_x in devices has been reported by many authors.^{19,33–35} Our experiment here also showed that the MoO_x films deposited on MAPbI₃ substrate in the vacuum was composed of Mo⁵⁺ and Mo⁶⁺. We took the thickness of

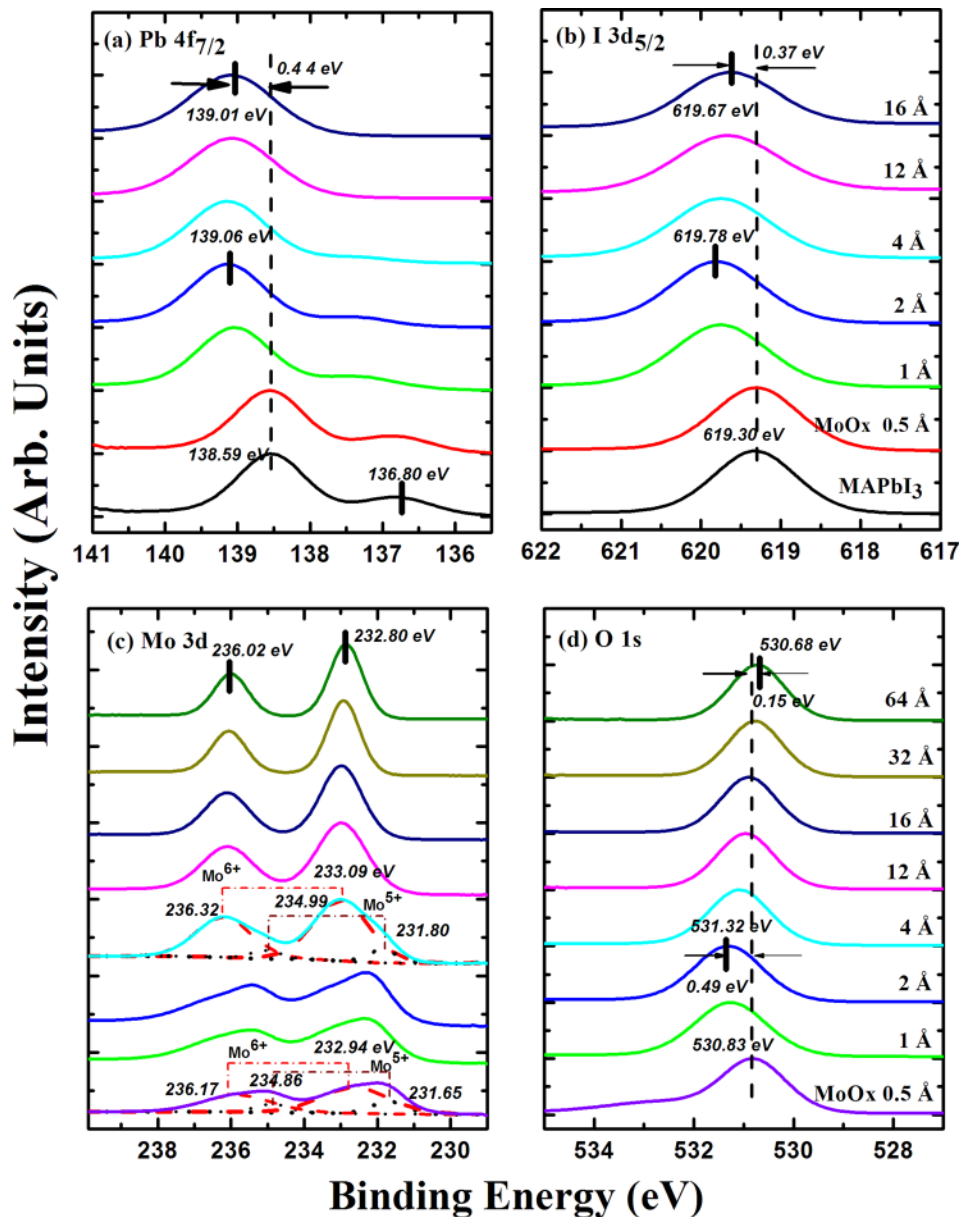


FIG. 2. XPS spectra of (a) Pb 4f_{7/2}, (b) I 3d_{5/2}, (c) Mo 3d, and (d) O 1s core levels of the MAPbI₃/MoO_x interface as a function of increasing MoO_x layers. The dashed line and dotted line in (c) are the fitting of the experimental data using Mo⁶⁺ and Mo⁵⁺ Gaussian components.

MoO_x films at 0.5 Å and 4 Å to reveal the evolution of oxides species. For the MoO_x coverage of 0.5 Å, Mo 3d core level contains a pair of main peaks with a ~3.2 eV spin-orbit splitting between them, the one centered on ~235.1 eV belongs to Mo 3d_{3/2}, and the other one centered on ~231.9 eV belongs to Mo 3d_{5/2}. A pair of shoulder peaks appear at about 1.3 eV higher binding energy than their main peaks, which means a single doublet could not resolve the observed XPS spectra. From a fitting analysis with a Gaussian/Lorentzian mixing function, the positions of Mo 3d_{5/2} of two oxidation states of Mo, Mo⁶⁺, and Mo⁵⁺, are measured to be 232.94 eV (see dashed line) and 231.65 eV (see dotted line), respectively. The corresponding energy differences between the peak of Mo⁶⁺ and the peak of Mo⁵⁺ and the peak of O 1s are 297.89 eV and 299.18 eV, respectively. The results agree well with our previous reports,^{26,36,37} in which the energy separations between the Mo 3d_{5/2} and O 1s are 297.8 eV and 299.1 eV for Mo⁶⁺ and Mo⁵⁺, respectively.

We focus on the peak of Mo⁶⁺ with respect to Mo 3d_{5/2} in Figure 2(c), the peak position shifts from 232.94 eV with the deposition of 0.5 Å MoO_x to slightly higher binding energy at low MoO_x deposition of up to 2 Å, which could be ascribed to the charging effect during the XPS measurement, then it turns to shift toward lower BE with following deposition of MoO_x showing a saturation of 232.80 eV with 64 Å MoO_x coverage, indicating a total shift of ~0.15 eV toward the E_F. As shown in Figure 2(d), the position of the O 1s peak shows an approximately same shift as the Mo⁶⁺ peak of Mo 3d_{5/2}. Therefore, a total band bending-up of ~0.15 eV in the MoO_x coverage is achieved with the MoO_x deposition of 64 Å. It is worth mentioning that this band bending-up is significantly smaller than the VBM shift upward of ~0.3 eV obtained by UPS in Figure 1(b). The difference of 0.15 eV between them can be most likely ascribed to the charging effect in XPS measurement, which is consistent with the result obtained by rectifying the core levels by reference to the C 1s of amorphous carbon. Therefore, the actual band bending-up of MoO_x film is ~0.30 eV after eliminating the charging effect. Similarly, in the underlying MAPbI₃ layer, the actual band bending-down should be ~0.25 eV after incorporating the charging effect into the shift of ~0.4 eV toward to higher band energy as shown in Figures 2(a) and 2(b).

The evolution of the ratio of Mo⁵⁺ to Mo⁶⁺ (Mo⁵⁺/Mo⁶⁺) is plotted in Figure 3(a) with increasing thickness of the MoO_x coverage. It is found that the fraction of Mo⁵⁺ is much less than that of Mo⁶⁺. At the MoO_x deposition of 0.5 Å, the Mo⁵⁺/Mo⁶⁺ ratio is about 0.24, then the fraction of Mo⁵⁺ begins to slightly increase accompanied with the decrease of Mo⁶⁺ with the following MoO_x deposition of up to 2 Å, leading to a slight increase of Mo⁵⁺/Mo⁶⁺. This may be due to electron transfer from perovskite to MoO_x. Such a transfer can lead I⁻ to neutral I, which subsequently leaves the surface because of the high vapor pressure as we discussed previously. Then, with the subsequent MoO_x deposition of up to 64 Å, the content of Mo⁵⁺ continuously decreases and only Mo⁶⁺ can be detected with the MoO_x deposition of beyond 12 Å. According to the change of intensity for Pb 4f_{7/2} and I 3d_{5/2}, we observed that I signal drops much quicker than Pb. This is an evidence to confirm that I is leaving during the MoO_x deposition. Actually, as shown in Figure 3(b), the ratio

of I to Pb (I/Pb) reduces from 2.15:1 of the pristine film to 0.67:1 after the deposition of 16 Å of MoO_x, indicating a significant deviation from the stoichiometry of MAPbI₃. Furthermore, the core levels of Mo 3d and O 1s shift to the opposite direction of I 3d and Pb 4f, a further evidence of perovskite decomposition in addition to the I:Pb ratio reduction. We obtained the ratios of Mo⁵⁺/Mo⁶⁺ and I/Pb based on the XPS data by using Gaussian/Lorentzian fitting and incorporating atomic sensitivity factors.

The energy levels alignment diagram for the MAPbI₃/MoO_x interface is shown in Figure 3(c). The band gap of MAPbI₃ is taken as 1.7 eV according to our previous results^{31,38} and the corresponding CBM of MAPbI₃ locates at ~0.30 eV above the E_F, which means the MAPbI₃ sample used here is heavily n-type material. The band gap of MoO_x is set as 3.2 eV by assuming the optical gap of MoO_x as the difference between its CB minimum and VBM. There is a band bending-down of 0.25 eV in the underlying MAPbI₃ layer, while a band bending-up of ~0.64 eV for the vacuum level and a band bending-up of ~0.30 eV for the VBM in the MoO_x overlayer with enough thickness of the MoO_x deposition. An interface dipole of ~2.13 eV observed at MAPbI₃/MoO_x interface can be attributed to the electron transfer from the lower WF material MAPbI₃ to the higher WF material MoO_x.

Given that MAPbI₃ is used as absorber layer to provide charge carriers in OPV devices, while MoO_x is used as anode buffer layer to efficiently enhance hole transport and suppress electron transport. Therefore, it is interesting to discuss the potential barrier of the MAPbI₃/MoO_x interface for hole and electron transfer. It is observed that there is a potential barrier of 1.36 eV for hole extraction from MAPbI₃ to MoO_x due to the offset between their VBMs, which will impede the hole extraction rather than enhance it. On the other hand, a small potential barrier of ~0.14 eV for electron extraction is achieved due to the offset between their CBMs, which is too low to suppress the electron extraction from MAPbI₃ to MoO_x. Therefore, we can conclude that such an interface does not provide a favorable energy level alignment to exclusively collect holes. Actually, the MAPbI₃/MoO_x interface is not an ideal choice for hole extraction in OPV devices. Some special hole transfer materials should be inserted between the MAPbI₃ layer and the MoO_x layer not only to achieve the favorable energy level alignment, thus to fulfill the Ohm contact, but also to suppress the chemical reaction between them.

In conclusion, we have investigated the interfacial electronic properties of the interface of MAPbI₃/MoO_x using UPS and XPS. The energy levels of MAPbI₃ shifted toward higher binding energy by 0.25 eV with the MoO_x overlayer of 64 Å upon it, which can be ascribed to the electron transfer from MAPbI₃ to MoO_x. Meanwhile, the energy levels of the MoO_x coverage shifted upward by 0.30 eV, and an interface dipole of ~2.13 eV was observed at the MAPbI₃/MoO_x interface. Most importantly, the chemical reaction taking place at such an interface, exemplified by the rapid reduction of iodine after MoO_x deposition, results in unfavorable interface energy level alignment for hole extraction. The potential barrier of 1.36 eV for hole extraction was too big to efficiently transfer holes from MAPbI₃ to MoO_x, while the

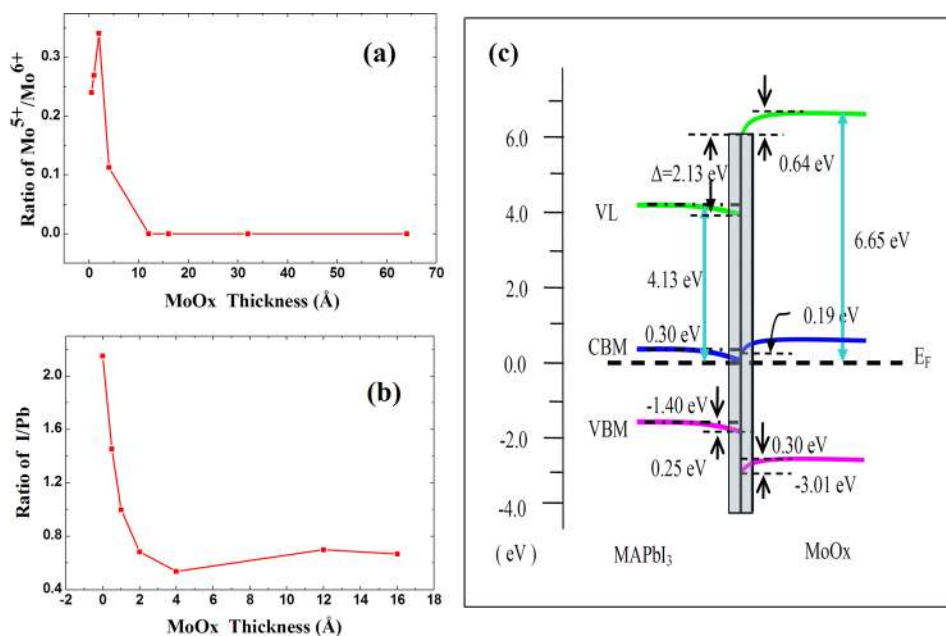


FIG. 3. The ratio of (a) Mo⁵⁺/Mo⁶⁺ and (b) I/Pb with increasing thickness of the MoO_x coverage. (c) The energy levels alignment diagram at the MAPbI₃/MoO_x interface.

potential barrier of ~ 0.14 eV for electron extraction was too small to efficiently suppress electrons extracted from MAPbI₃ to MoO_x. Therefore, it is concluded that the MAPbI₃/MoO_x interface is not an ideal choice for hole extraction in OPV devices.

We thank the financial support by the National Science Foundation (Grant No. CBET-1437656) and the National Natural Science Foundation of China (Grant Nos. 51173205 and 11334014). J. Huang thanks the financial support by the National Science Foundation under Award Nos. ECCS-1252623 and ECCS-1201384, and Defense Threat Reduction Agency under Award No. HDTRA1-14-1-0030.

¹M. A. Green, A. Ho-Baillie, and H. J. Snaith, *Nat. Photonics* **8**, 506 (2014).
²N. J. Jeon, J. H. Noh, Y. C. Kim, W. S. Yang, S. Ryu, and S. Seok, *Nat. Mater.* **13**, 897 (2014).
³N. J. Jeon, J. H. Noh, W. S. Yang, Y. C. Kim, S. Ryu, J. Seo, and S. Seok, *Nature* **517**, 476 (2015).
⁴J.-H. Im, I.-H. Jang, N. Pellet, M. Grätzel, and N.-G. Park, *Nat. Nanotechnol.* **9**, 927 (2014).
⁵Z. G. Xiao, Y. B. Yuan, Y. C. Shao, Q. Wang, Q. F. Dong, C. Bi, P. Sharma, A. Gruverman, and J. S. Huang, *Nat. Mater.* **14**, 193 (2015).
⁶J. Burschka, N. Pellet, S.-J. Moon, R. Humphry-Baker, P. Gao, M. K. Nazeeruddin, and M. Grätzel, *Nature* **499**, 316 (2013).
⁷M. Liu, M. B. Johnston, and H. J. Snaith, *Nature* **501**, 395 (2013).
⁸D. Liu and T. L. Kelly, *Nat. Photonics* **8**, 133 (2014).
⁹A. Kojima, K. Teshima, Y. Shirai, and T. Miyasaka, *J. Am. Chem. Soc.* **131**, 6050 (2009).
¹⁰U. Bach, D. Lupo, P. Comte, J. E. Moser, F. Weissortel, J. Salbeck, H. Spreitzer, and M. Grätzel, *Nature* **395**, 583 (1998).
¹¹J. M. Ball, M. M. Lee, A. Hey, and H. J. Snaith, *Energy Environ. Sci.* **6**, 1739 (2013).
¹²H. Zhou, Q. Chen, G. Li, S. Luo, T.-B. Song, H.-S. Duan, Z. Hong, J. You, Y. Liu, and Y. Yang, *Science* **345**, 542 (2014).
¹³S. D. Stranks, G. E. Eperon, G. Grancini, C. Menelaou, M. J. P. Alcocer, T. Leijtens, L. M. Herz, A. Petrozza, and H. J. Snaith, *Science* **342**, 341 (2013).
¹⁴Q. Dong, Y. Fang, Y. Shao, P. Mulligan, J. Qiu, L. Cao, and J. Huang, *Science* **347**, 967 (2015).
¹⁵J. Meyer, K. Zildberger, T. Riedl, and A. Kahn, *J. Appl. Phys.* **110**, 033710 (2011).

¹⁶V. Shrotriya, G. Li, Y. Yao, C. W. Chu, and Y. Yang, *Appl. Phys. Lett.* **88**, 073508 (2006).
¹⁷H. Wang, Z. Liu, M. F. Lo, T. W. Ng, C.-S. Lee, D. Yan, and S.-T. Lee, *J. Appl. Phys.* **107**, 024510 (2010).
¹⁸Irfan, M. Zhang, H. Ding, C. W. Tang, and Y. Gao, *Org. Electron.* **12**, 1588 (2011).
¹⁹X. L. Liu, C. G. Wang, I. Irfan, S. J. Yi, and Y. Gao, *Org. Electron.* **15**, 977 (2014).
²⁰X. Liu, S. Yi, C. Wang, C. Wang, and Y. Gao, *J. Appl. Phys.* **115**, 163708 (2014).
²¹S. Tokito, K. Noda, and Y. Taga, *J. Phys. D: Appl. Phys.* **29**, 2750 (1996).
²²X. L. Liu, C. G. Wang, C. C. Wang, I. Irfan, and Y. Gao, *Org. Electron.* **17**, 325 (2015).
²³J. Hou, J. Wu, Z. Xie, and L. Wang, *Appl. Phys. Lett.* **95**, 203508 (2009).
²⁴M. Kröger, S. Hamwi, J. Meyer, T. Riedl, W. Kowalsky, and A. Kahn, *Appl. Phys. Lett.* **95**, 123301 (2009).
²⁵Y. Nakayama, K. Morii, Y. Suzuki, H. Machida, S. Kera, N. Ueno, H. Kitagawa, Y. Noguchi, and H. Ishii, *Adv. Funct. Mater.* **19**, 3746 (2009).
²⁶C. Wang, I. Irfan, X. Liu, and Y. Gao, *J. Vac. Sci. Technol., B* **32**, 040801 (2014).
²⁷M. Zhang, Irfan, H. Ding, Y. Gao, and C. W. Tang, *Appl. Phys. Lett.* **96**, 183301 (2010).
²⁸Q. Wang, Y. Shao, H. P. Xie, L. Lyu, X. Liu, Y. Gao, and J. Huang, *Appl. Phys. Lett.* **105**, 163508 (2014).
²⁹Z. Xiao, C. Bi, Y. Shao, Q. Dong, Q. Wang, Y. Yuan, C. Wang, Y. Gao, and J. Huang, *Energy Environ. Sci.* **7**, 2619 (2014).
³⁰P. Schulz, E. Edri, S. Kirmayer, G. Hodes, D. Cahen, and A. Kahn, *Energy Environ. Sci.* **7**, 1377 (2014).
³¹R. Lindblad, D. Bi, B. Park, J. Oscarsson, M. Gorgoi, H. Siegbahn, M. Odelius, E. M. J. Johansson, and H. Rensmo, *J. Phys. Chem. Lett.* **5**, 648 (2014).
³²M. Kröger, S. Hamwi, J. Meyer, T. Riedl, W. Kowalsky, and A. Kahn, *Org. Electron.* **10**, 932 (2009).
³³M. P. Ramuz, M. Vosgueritchian, P. Wei, C. Wang, Y. Gao, Y. Wu, Y. Chen, and Z. Bao, *ACS Nano* **6**, 10384 (2012).
³⁴M. Vasilopoulou, L. C. Palilis, D. G. Georgiadou, P. Argitis, S. Kennou, L. Sygellou, I. Kostis, G. Papadimitropoulos, N. Konofaos, A. A. Iliadis, and D. Davazoglou, *Appl. Phys. Lett.* **98**, 123301 (2011).
³⁵M. T. Greiner, M. G. Helander, Z. B. Wang, W. M. Tang, J. Qiu, and Z. H. Lu, *Appl. Phys. Lett.* **96**, 213302 (2010).
³⁶C. Wang, A. J. Turinske, and Y. Gao, *Appl. Phys. B* **113**, 361 (2013).
³⁷I. Irfan and Y. Gao, *J. Photonics Energy* **2**, 021213 (2012).
³⁸X. L. Liu, C. G. Wang, L. Lyu, C. C. Wang, Z. G. Xiao, C. Bi, J. S. Huang, and Y. Gao, *Phys. Chem. Chem. Phys.* **17**, 896–902 (2015).